JOURNAL OF AGRICULTURAL AND FOOD CHEMISTRY

Magnetic Resonance Imaging for Nondestructive Analysis of Wine Grapes

JORGE E. ANDAUR,[†] ANDRÉS R. GUESALAGA,*[,†] EDUARDO E. AGOSIN,[§] MARCELO W. GUARINI,[†] AND PABLO IRARRÁZAVAL[†]

Pontificia Universidad Católica de Chile, Avenida Vicuña Mackenna 4860, Macul, Santiago, Chile

Magnetic resonance imaging (MRI) was used to study the growth and ripening of grape berries for three varieties. The results show that this technique allows the visualization of internal characteristics of berries using noninvasive procedures in order to obtain the volume and °Brix distribution within a cluster. Samples of Cabernet Sauvignon, Carmenère, and Chardonnay varieties collected over the 2002 season were analyzed. Calibration models were developed to correlate soluble solids (°Brix) against spin−lattice relaxation time t_1 and spin−spin relaxation time t_2. The correlation of °Brix and t_1 was $R^2 = 0.75$ for Cabernet Sauvignon, $R^2 = 0.8$ for Carmenère, and $R^2 = 0.65$ for Chardonnay. In the case of t_2 the correlation was significantly lower. Reconstruction techniques for the three-dimensional representation of clusters were developed, allowing an interactive visualization of the bunches. The method also provides volume measurements of single berries and their distribution within the cluster with an accuracy of 3% and $R^2 = 0.98$. These results show the potential of MRI in the wine industry for both monitoring and research. Not only does it provide quantitative information about the berries such as volume and °Brix distributions, but it can also be used to support the sampling procedures by providing a better cluster characterization.

KEYWORDS: Magnetic resonance imaging; wine grapes; ripeness; °Brix

INTRODUCTION

The growth of a grape berry consists of two successive sigmoid cycles separated by a lag phase (*1*). In the first stage, the berry is hard and green with a slow growth rate. The second cycle begins with the onset of sugar accumulation, berry softening and coloring, and renewed size increase. This process is known as *veraison*, constituting the early stages in the grape ripening (*2*).

The criteria used to determine grape maturity are based on the sugar content of the berry, its acidity, color, and varietal fruitiness (*3*).

The sugar content or its accumulation in a berry is normally measured in °Brix units using densitometry or refractometry. High values of soluble solids (°Brix) indicate a high degree of ripeness, which normally ceases at about 25−26 °Brix in the late stages of ripening (*4*). Sugar alone, however, is not a fully adequate criteria for harvesting wine grapes, and other factors such as acidity, weight, anthocyanins, tannins, and total phenolic content are also important criteria that support the moment for harvesting (*3*, *5*).

According to Kennedy (*6*), red wine producers favor small berries with a high skin-to-flesh ratio, because the majority of components that define the color (anthocyanins) and flavors are located in the skin of the fruit.

In terms of volume, berry size increases according to the number of seeds per berry in a larger proportion than their sole weight. This fact becomes important in wines where extraction is present, because in the case of phenols, for instance, only ∼10% of these constituents are present in the juice, whereas 30% are in the skin and 60% are in the seeds of seeded varieties (*3*).

This implies that the volume of berries and their numbers of seeds and skin-to-flesh ratios are also important variables to track.

Magnetic resonance imaging (MRI), based on the principles of nuclear magnetic resonance (NMR), has achieved general acceptance as a powerful medical imaging tool. For a detailed description of the technique, the reader is referred to McCarthy (*7*), Liang and Lauterbur (*8*), and Kuperman (*9*).

The noninvasive, nondestructive attributes of MRI, and its ability to provide highly resolved spatial information about the density of hydrogen (or other atoms) and their magnetic spin relaxation properties in soft tissues, make it an attractive technique for physiological research on fruits and vegetables (*10*).

MRI signals are sensitive to the inherent properties of the sample and to the experimental settings. MR images are two-dimensional arrays of signal intensities from small discrete volumes inside the sample. The array elements are called pixels,

* Author to whom correspondence should be addressed [telephone (56-2) 686 4282; fax (56-2) 552 2563; e-mail aguesala@ing.puc.cl].
[†] Department of Electrical Engineering.
[§] Department of Chemical and Bioprocesses Engineering.

10.1021/jf034886c CCC: $27.50
Published on Web 12/17/2003

and the signal intensity of each pixel is influenced by nuclear spin density ρ, the spin−lattice relaxation time t_1, the spin−spin relaxation time t_2, molecular motion, susceptibility effects, and chemical shift differences. The imaging effects of these parameters can be suppressed or enhanced in a specific experiment by operator-selectable parameters, such as repetition time t_R, echo time t_E, recovery time t_I, and flip angle α.

The estimation of relaxation times can provide insight information of the molecular structures in soft tissues, and evidence also suggests that they can reflect physiological changes in fruit during ripening (*11*−*15*).

Exploiting particular pulse sequences or operator-selectable parameters (t_E and t_R) to highlight tissues in two-dimensional (2D) images offers some interesting possibilities when extended to three dimensions. For example, the 3D image reconstruction of intact fruits (mango and papaya) can provide information on the total volume (*16*). Another application to fruit analysis is found in ref *17*, where physiological disorders in apples such as watercore and browning are studied. Glidewell et al. (*18*) used surface rendering to determine the 3D histology of seeds in intact grape berries using magnetic resonance microscopy.

This study evaluates the potential of MRI as a nondestructive technique to characterize the spatial and temporal growth and ripening of wine grapes.

Models for spatial characterization of clusters in terms of sugar content (°Brix) and distribution of berry volumes within clusters were calibrated and validated.

MATERIALS AND METHODS

Samples. Samples of three varieties of wine grapes (Cabernet Sauvignon, Carmenère, and Chardonnay) were collected during the months of February, March, and April 2002. The selected vineyard was located at Maipo Valley (Concha y Toro winery), Chile. For each variety, three clusters were collected twice a week. After harvesting, 30% of the samples were immediately processed and the other 70% were frozen at −20 °C for later analysis.

Hardware. The MRI scanner used in this research is a Phillips T5-Intera of 0.5 T with a head coil of 28 cm in diameter and 30 cm long. It is located at the Magnetic Resonance Research Center (www.mri.cl) in San Joaquín Medical Center of the Pontificia Universidad Católica in Santiago, Chile.

Reference values for calibration of °Brix models were obtained using a CETI Digit-032 refractometer. For volume reference values, a Mitutoyo Vernier caliper with a reading error of 0.05 mm was used.

Software. Specific functions were developed in Matlab 6.1 in order to process the images in DICOM format obtained from the MRI scanner. Matlab graphic tools were also used to display the objects using 3D models constructed through isosurfaces to show the overall structure of the cluster together with the isocaps to reveal information about the interior of 2D slices. The software allows the visualization of the cluster for different slice orientations, together with calculations performed on a particular cut, such as °Brix and volume distribution of the berries.

Experiments. Clusters were scanned as quickly as possible to reduce changes in their chemical properties. When they could not be analyzed within the same day due to scanner availability, they were frozen and stored for later processing. Frozen samples were thawed prior to scanning. Tests were carried out to check the validity of this procedure, and no changes were found in sugar content for the same samples analyzed before and after freezing. For volume estimation there was a significant change in the berry shape and volume, so only fresh clusters were used for this purpose.

The first experiment was carried out to calibrate a model for °Brix and relaxation time t_1. Twelve clusters of each variety were processed. Fifteen berries were selected in each cluster, choosing five from the top, five from the middle, and five from the bottom of the bunch, including samples from both the surface and the interior of the cluster.

Table 1. MRI Protocol Parameter Used for the First Experiment

protocol parameter	value
scan mode	multislice
scan technique	inversion recovery
FOV (mm)	180
matrix scan	256 × 256
t_R (ms)	7000.00
t_E (ms)	20.00
IR delay (ms)	50–200–350–500–750–1000–1500–2000–3000
slice thickness (mm)	2.00
slice gap (mm)	0.00
no. of averages	2

Images with a resolution of 256 × 256 pixels were acquired, using a field of view of 180 mm and a slice thickness of 2 mm.

Maps of t_1 were constructed to determine the localized relaxation times within the bunch. For each map generation, nine t_1-weighted images were acquired with t_I values of 50, 200, 350, 500, 750, 1000, 1500, 2000, and 3000 ms. These values were selected after several alternatives had been tried. Parameter t_R was set to 7 s, 5 times larger than the maximum t_1 obtained for the berries under analysis (1.4 s). t_E was set to 20 ms. **Table 1** summarizes the protocol parameters used in this first experiment.

On the basis of eq 1, a nonlinear regression was performed on the images in order to estimate t_1 for each pixel.

$$I_{IR}(x,y) = K\rho(x,y)[1 - 2e^{(-t_I/t_1(x,y))}] \quad (1)$$

Once the maps of t_1 had been generated, pixels associated with berry flesh were identified and isolated for analysis. This segmentation was carried out using a watershed segmentation algorithm (*19*). Care was taken to avoid pixels containing seeds or skin, as this proved to distort the measurements. After estimation of t_1 for every pixel in a berry, their mean value was calculated.

The second experiment consisted of taking spatial information from berries in order to reconstruct 3D models of the fruit. This was done by piling up a group of slices with 2 mm thickness for the sample set in the previous experiment.

In this set of images, a spin−echo sequence with $t_R = 4$ s and $t_E = 20$ ms was used to obtain good signal-to-noise ratios, taking advantage of the high proton density in berries due to their high water content. These parameters generated significant reductions of t_1 and t_2 contrasts between consecutive acquisitions.

This set of slices was also used to calibrate a model for the volume measurement of berries. The reference value used to perform the calibration was a caliper that measures the diameter of the berry, and because the berries have a shape close to a sphere in the three varieties under analysis, the volume was calculated using the equatorial radius (*20*).

The roundness of the berry was verified in the slices scanned (radius in *X* axis equals that in *Y*). However, this does not apply in the *Z* axis, because the resolution in this axis is given by the number of slices considered. An integration of the volume between slices had to be performed for the 2 mm separation. This was done by taking an adjacent slice for the calculation. Using simulation, it was found that a good estimation of the volume contained between two cuts is

$$V = \theta r_1^2 \pi h + (1 - \theta) r_2^2 \pi h \quad (2)$$

where r_1 is the radius of the largest slice scanned and r_2 the radius of the smaller one (**Figure 1**). Parameter h is the slice separation (2 mm), and θ is a calibration parameter found via simulations that weigh the two slices. In this case, $\theta = 0.66$.

The next step in the development of analysis tools was the integration of the previous experiments to study the complete cluster. The goal sought was the spatial characterization of the cluster in terms of volume and °Brix variables. The result allows the visualization of spatial distribution of these variables.

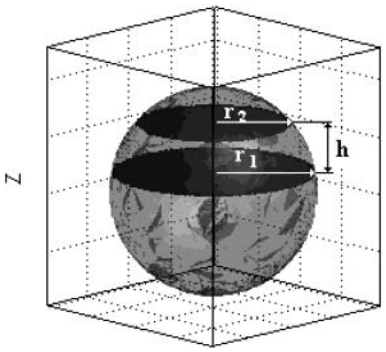

Figure 1. Circles of scanned slices used to calculate volume portions.

Table 2. Summary of °Brix Values Using a Refractometer

variety	mean	SD	max	min
Carmenère	19.6	3.98	27.1	10.3
Cabernet Sauvignon	22.4	3.8	29.5	13
Chardonnay	21.8	2.47	25.8	14

For this integrated approach, we first scan the cluster via slices to obtain its 3D reconstruction and volume distribution. Parallel slices with a separation of 2 mm were acquired. A spin−echo sequence with $t_R = 4$ s and $t_E = 20$ ms (proton-weighted images) was used. The total number of slices, *n*, was then determined according to the size of the cluster. Maps for t_1 and t_2 were also constructed for some slices to study the distribution of °Brix within the bunch.

RESULTS AND DISCUSSION

In the first experiment, the °Brix reference values of berry used for calibration were directly obtained using refractometry (**Table 2**).

Correlations between the measured relaxation times and °Brix values were obtained for the three varieties under study. **Figure 2** shows the model adjusted for Carmenère. The calibrations obtained for t_1, using a linear regression, are represented by the solid line.

The calibration parameters for the three varieties studied are summarized in **Table 3**. The comparison of the results was made in terms of R^2 (coefficient of determination) and SE_{est} (standard error of estimation).

For each set of samples, ∼25% of them were separated for later validation. This subset was selected randomly but uniformly over the full range of °Brix values. The validation parameters for the three varieties studied are summarized in **Table 4**.

The results show a good correlation between t_1 and °Brix, especially for the red varieties. For Chardonnay, the correlation is lower, but still worth considering. In the case of t_2, the correlation is not important and no significant information can be expected from this variable. As expected, the calibration in terms of SE_{est} is also better for t_1.

Notice that shorter relaxation times are associated with increasing solid soluble concentration. This is consistent with the results reported by Arulmozhi and Srinivasa (*21*) and Sattiacoumar and Arulmozhi (*22*), who measured spin−lattice relaxation times (t_1) in aqueous solutions of glucose and sucrose and found that t_1 decreased for higher concentrations of sugar, reflecting the molecular interaction between sugar and water molecules. This relationship has also been suggested by Cho et al. (*23*), who established a negative correlation between relaxation times and soluble solids using a theoretical model.

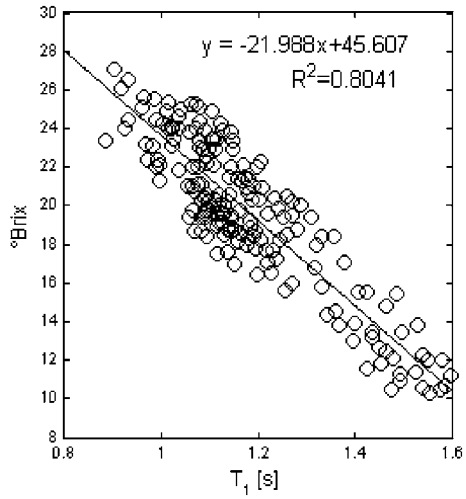

Figure 2. Correlation of °Brix and relaxation time t_1 for Carmenère variety. The solid line shows the calibrated model.

Table 3. Summary of Calibration of °Brix Using Relaxation Times t_1 and t_2

variety	R^2 (t_1)	SE_{est} (t_1)	R^2 (t_2)	SE_{est} (t_2)
Carmenère	0.8041	1.76	0.5129	3.38
Cabernet Sauvignon	0.7531	1.88	0.4223	2.88
Chardonnay	0.6519	1.45	0.3184	2.03

Table 4. Summary of Validation Results

variety	R_v^2 (t_1)	SE_{est} (t_1)	R_v^2 (t_2)	SE_{est} (t_2)
Carmenère	0.7948	1.93	0.4101	3.67
Cabernet Sauvignon	0.7124	1.96	0.4646	2.62
Chardonnay	0.6746	1.45	0.3578	2.04

In transverse relaxation (t_2) the results showed high SE_{est} values, not practical for °Brix estimation. A possible reason for this insensitivity is the effect of diffusion in a pulse sequence like t_2−spin−echo, where for a short value of TE, the effect of diffusion is small. However, as TE becomes large, the diffusion attenuation can become quite large, affecting the precise measurement of the t_2 constant.

According to Clark et al. (*10*), the inherent variability in structure and composition of some fruits makes it difficult to establish consistent associations between the relaxation times and soluble solids in the general case. This consideration, together with the differences found among the varieties studied, suggests that the model could be improved by introducing additional terms in the calibration.

One of the interesting results obtained with this calibration refers to the homogeneity of the sugar content inside the berry. **Figure 3** shows the spatial distribution of this variables in terms of °Brix for the valid pixels contained in a berry. Notice the low deviations in °Brix values among pixels.

Next, a calibration for the estimation of the berry volume was carried out, obtaining an average of 3.15% for the absolute error, with a standard deviation of 2.14%. In terms of R^2, the value was 0.9825 (**Figure 4**). The method determines the size distribution of berries with a reasonable accuracy. The size distribution of berries is important when one is trying to predict extractability in grapes, because this characteristic is a function of the skin-to-flesh ratio and hence inversely proportional to the volume of the berries (*6*).

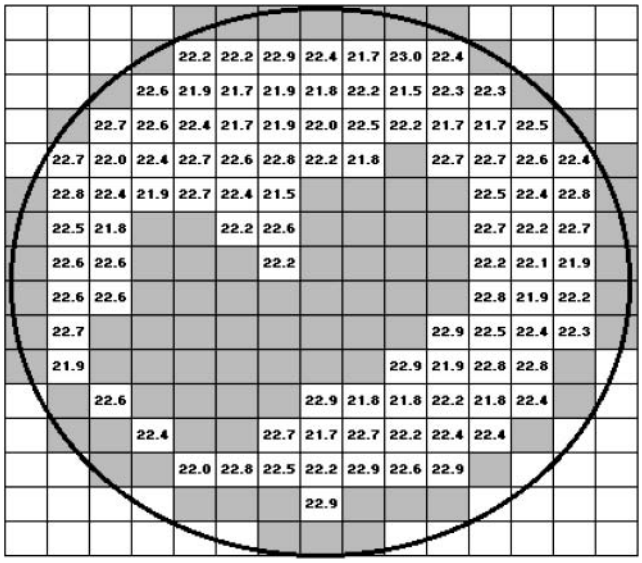

Figure 3. Sugar content (°Brix) of the selected pixels in a berry.

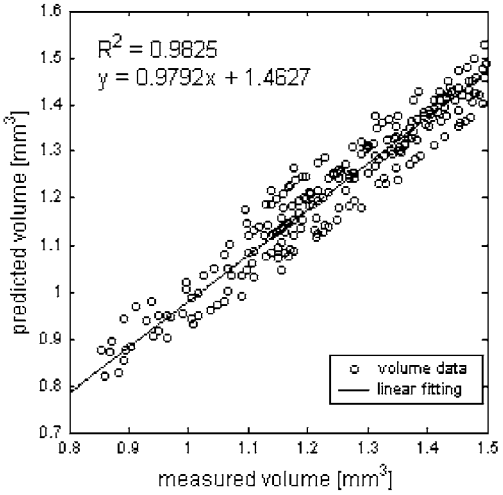

Figure 4. Correlation between measured and predicted berry volume. The solid line shows the calibrated model.

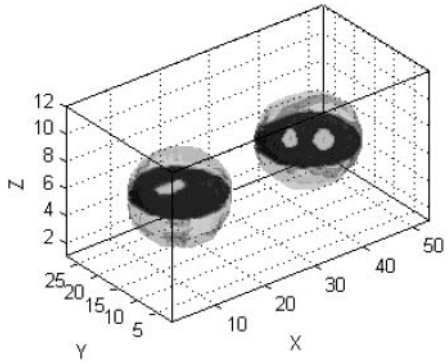

Figure 5. Internal structure visualization of a berry. Characteristics such as seeds and seed size are clearly seen.

The technique was also assessed for its ability to provide nondestructive information about the internal structure of the berry. **Figure 5** shows the potential of this visualization, where characteristics of berries such as seeds and seed size are clearly seen. This can be of great importance in the estimation of tannin impact on wine astringency (*6*).

Analysis of individual berries can also be applied to complete clusters. **Figure 6a** shows a 3D model of a cluster, giving a rapid overall view of the bunch structure, as well as a spatial distribution of variables associated with the berries that form the cluster. Variables such as the number of berries and seeds in a cluster can be determined quantitatively (**Figure 6b**).

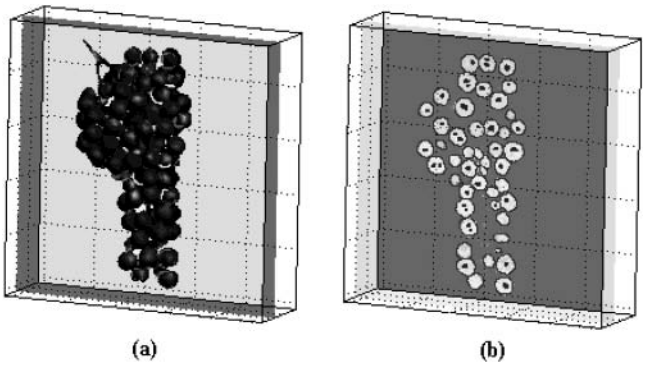

Figure 6. Internal visualization of the cluster: (**a**) slice selection within the cluster; (**b**) internal visualization of the slice reveals seed distribution in the bunch.

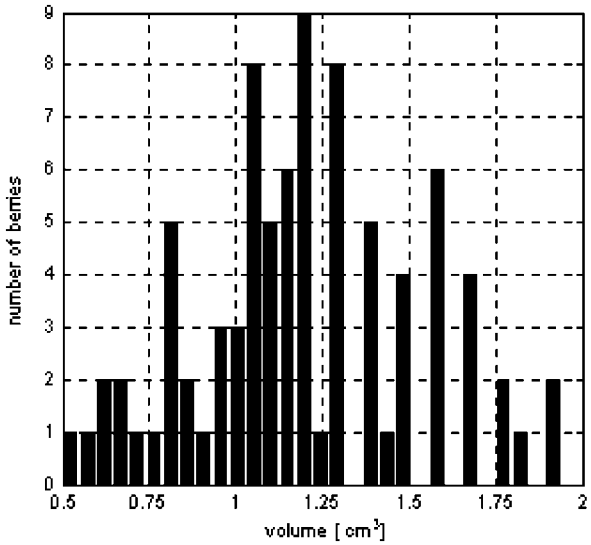

Figure 7. Berry volume distribution within a cluster. Partitions of 0.05 cm^3 have been used.

To determine the size distribution of the berries, the technique can generate histograms showing the number of berries for different size ranges (**Figure 7**).

The technique provides a way to estimate the sugar distribution (°Brix) within the cluster. **Figure 8** shows a horizontal slice of the cluster with the sugar content represented in different shading intensities. The map is constructed following the steps described previously. Care had to be taken to reject pixels that were not completely contained in the berry or those having parts of a seed, because it was found that in these cases, significant errors could be induced in the calculations. To achieve this selection, the berries were first identified together with the pixels contained inside them. Each pixel intensity and relaxation time t_1 was compared to the average values of the other pixels in the berry. The highly homogeneous characteristic of sugar within the fruit, as exemplified by **Figure 3**, make this simple approach very effective. **Figure 8** clearly suggests that a nonrandom distribution of °Brix exists within the cluster. Spatial orientation of the cluster before harvesting is needed to take full advantage of this tool, because it could yield to conclusions on the effect of variables such as illumination or humidity on grape ripening (*24*). This is of great importance for cluster modeling when sampling strategies are designed.

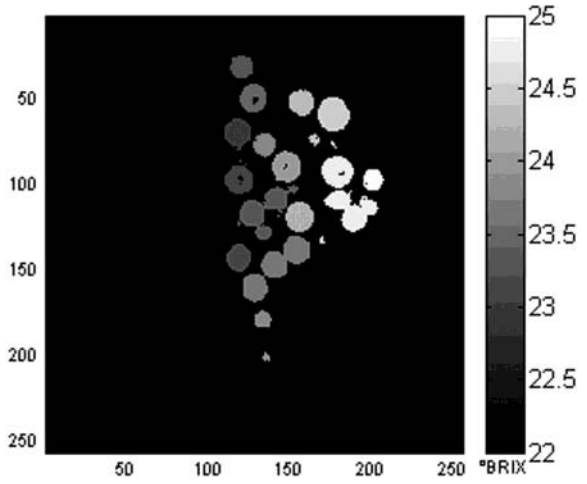

Figure 8. Sugar distribution (°Brix) of a horizontal slice of a cluster. Sugar content is shown as different intensities of shading.

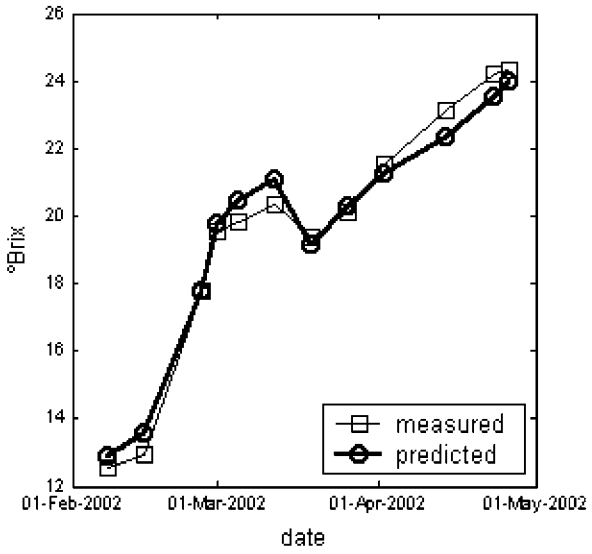

Figure 9. Carmenère time evolution of °Brix (refractometry has been used for measured values).

Another analysis of grape ripening, such as the classical evolution of °Brix for berries located in a given part of the cluster, can be carried out. **Figure 9** shows the measured and predicted values of °Brix (Carmenère) for three months starting in February. This could be used, for instance, to model the ripening process of berries located in certain parts of the cluster.

The heavy line represents the predicted values obtained from the calibrated models for the complete set of scanned samples, whereas the lighter line shows the refractometry measurements. It can be seen that a fairly good match is obtained for the estimation of the ripeness of the samples. The lower accuracy obtained for the white variety could be explained by the influence of organic acids on the relaxation time t_1 at the early stages of the sampling process.

CONCLUSIONS

A clinical scanner has been used to explore the possibilities of MRI in the analysis of wine grapes. The equipment has been used for exploration purposes, and this study does not pretend to demonstrate its usage on a daily basis. It is important to mention that the required field of view to accommodate the complete clusters could not be easily found in other similar equipment such as NMR spectrometers that use higher fields but smaller bores.

The results obtained in this work show the potential of MRI as a tool for off-line analysis of wine grapes. Due to its nondestructive nature, it can provide rapid information about the physical ripening of individual berries or clusters. Standard laboratory analysis of a cluster could take hours if spatial distribution of sugar content and size are to be measured. Using this technique, the time required to obtain such information is reduced to the scanning time, typically 20−30 min.

Spatial distribution of variables such as berry size, °Brix, and number of seeds can also be a powerful tool for winemakers.

The search for correlations with parameters other than °Brix should be addressed to expand the possibilities of the technique.

This powerful tool can be used in grape modeling and when sampling strategies in vineyards are defined. The ability to relate certain maturity variables of berries to their spatial location in the cluster or plant in a nondestructive way is unique.

Further work is required to enhance calibration with samples obtained from the next season and to verify the effect of geographical incidence in the models.

Localized spectroscopy and chemical shift imaging should also be considered in future work. This could allow the direct measurement of carbohydrates instead of inferring their presence on the basis of relaxation times. Use of surface coils to generate homogeneous magnetic fields in particular regions of the sample and analyzing the sugar/water ratio of their respective peaks based on the work by Zion et al. (*25*) is also pending.

A 2D spin−echo sequence was used due to its simplicity in acquisition and later processing; however, future work should consider a 3D sequence instead. The latter would give better signal-to-noise ratios, and the problem of filling the gaps between slices would be avoided.

Previous work on apple quality (*15*) has shown that a correlation exists between the self-diffusion coefficient (D) and the soluble solids content using NMR techniques ($R^2 = 0.68$). The application of these results to wine grapes should be considered in future work.

LITERATURE CITED

(1) Coombe, B. G. Research on development and ripening of the grape berry. *Am. J. Enol. Vitic.* **1992**, *43*, 101−110.
(2) Coombe, B. G.; McCarthy, M. G. Dynamics of grape berry growth and physiology of ripening. *Aust. J. Grape Wine Res.* **2000**, *6*, 131−127.
(3) Boulton, R. B.; Singleton, V. L.; Bisson, L. F.; Kunkee, R. E. Viticulture for winemakers. *Principles and Practices of Winemaking*; Chapman and Hall: New York, 1996; pp 13−61.
(4) Singleton, V. L. The total phenolic content of grape berries during the maturation of several varieties. *Am. J. Enol. Vitic.* **1966**, *17*, 126−134.
(5) Blouin, J.; Guimberteau, G. *Maturation et Maturité des Raisins*; Féret: Bordeaux, France, 2000.
(6) Kennedy, J. Understanding grape berry development. *Practical Winery Vineyard* **2002**, July/Aug, 14−18.
(7) McCarthy, M. J. *Magnetic Resonance Imaging in Foods*; Chapman and Hall: London, U.K., 1994.
(8) Liang, Z. P.; Lauterbur, P. C. *Principles of Magnetic Resonance Imaging. A Signal Processing Perspective*; Institute of Electrical and Electronics Engineers: New York, 2000.
(9) Kuperman, V. *Magnetic Resonance Imaging. Physical Principles and Applications*; Academic Press: San Diego, CA, 2000.
(10) Clark, C. J.; Hockings, P. D.; Joyce, D. C.; Mazucco, R. A. Application of magnetic resonance imaging to pre- and post-harvest studies of fruits and vegetables. *Postharvest Biol. Technol.* **1997**, *11*, 1−21.

(11) Callaghan, P. T.; Clark, C. J.; Forde, L. C. Use of static and dynamic NMR microscopy to investigate the origins of contrast in images of biological tissues. *Biophys. Chem.* **1994**, *50*, 225−235.

(12) Clark, C. J.; Drummond, L. N.; MacFall, J. S. Quantitative magnetic resonance imaging of kiwifruit during growth and ripening. *J. Sci. Food Agric.* **1998**, *78*, 349−358.

(13) Goodman, B. A.; Williamson, B.; Simpson, E. J.; Chudek, J. A.; Hunter, G.; Prior, D. A. M. High field NMR microscopic imaging of cultivated strawberry fruit. *Magn. Res. Imaging* **1996**, *14*, 187−196.

(14) Ishida, N.; Koizumi, M.; Kano, H. Ontogenetic changes in water in cherry tomato fruits measured by nuclear magnetic resonance imaging. *Sci. Hortic.* **1994**, *57*, 335−346.

(15) Keener, K. M.; Stroshine, R. L.; Nyenhuis, J. A. Evaluation of low field (5.40-mHz) proton magnetic resonance measurement of D_w and T_2 as methods of nondestructive quality evaluation of apples. *J. Am. Soc. Hortic. Sci.* **1999**, *124*, 289−295.

(16) Minghim, R.; Nonato, L. G.; Batista, J. E. S.; Biscegli, C. I.; Franco, R. W. A.; Jorge, L. A. C. Three-dimensional reconstruction of magnetic resonance images of mango and papaya. *Proceedings of the World Congress of Computers in Agriculture and Natural Resources*, Iguazu Falls, Brazil, 2002; American Society of Engineers: St. Joseph, Michigan, 2002; pp 86−92.

(17) Gonzales, J. J.; Valle, R. C.; Bobroff, S.; Biasi, W. V.; Mitcham, E. J.; McCarthy, M. J. Detection and monitoring of internal browing development in 'fuji' apples using MRI. *Postharvest Biol. Technol.* **2001**, *22*, 179−188.

(18) Glidewell, S. M. B.; Williamson, J. A.; Chudek, G.; Hunter, R. J.; McNicol; Goodman, B. A. Determination of 3-dimensional histology of grape seeds using NMR microscopic techniques. *Abstract of the 3rd International Conference on Magnetic Resonance Microscopy*, Wurzburg, Germany, 1995; German Cancer Research Center: Heidelberg, Germany, 1995; p 134.

(19) Sijbers, J.; Verhoye, M.; Scheunders, P.; Van der Linder, A. Watershed-based segmentation of 3d MR data for volume quantization. *Magn. Reson. Imaging* **1997**, *15*, 679−688.

(20) Dreier, L. P.; Stoll, G. S.; Ruffner, H. P. Berry ripening and evapotranspiration in *Vitis vinifera* L. *Am. J. Enol. Vitic.* **2000**, *51*, 340−346.

(21) Arulmozhi, V.; Srinivasa, A. Proton magnetic resonance relaxation studies in aqueous solutions of alkali halides and sugars. *Phys. Chem. Liq.* **1993**, *26*, 201−207.

(22) Sattiacoumar, S.; Arulmozhi, V. Proton NMR relaxation studies in aqueous solutions of sugars with alkali halides. *Bull. Soc. Chim. Belg.* **1993**, 102.

(23) Cho, S. I.; Stroshine, R. L.; Baianu, I. C.; Krutz, G. W. Nondestructive sugar content measurements of intact fruit using spin−spin relaxation time (T_2) measurements by pulsed ^1H magnetic resonance. *Trans. ASAE* **1993**, *36*, 1217−1221.

(24) Glynn, M. C. Distribution of °Brix, berry weight, seed number, anthocyanins, total skin phenols, skin hydroxycinnamates, and skin flavonols in a cabernet sauvignon cluster. M.S. Thesis, University of California, Davis, 2002.

(25) Zion, B.; Chen, P.; McCarthy, M. J. Non-destructive quality evaluation of fresh prunes by NMR spectroscopy. *J. Sci. Food Agric.* **1995**, *67*, 423−429.

Received for review August 4, 2003. Revised manuscript received November 6, 2003. Accepted November 9, 2003. We thank FONDECYT 1030562, FONDEF D00I1013, and MRI-Chile for sponsoring this project.

JF034886C